Development of Vessel Phantoms for Ultrasound Methods

Benjamin Meirza

LUND
UNIVERSITY

Master Thesis In
Biomedical Engineering

Faculty of Engineering LTH
Department of Biomedical Engineering

Supervisor: Magnus Cinthio
Assistant Supervisors: Maria Evertsson and Sandra Sjöstrand

To all mothers in the world for their endless patience

"Everything is possible until proven impossible, and then you just need to become more creative."
Scott Parazynski, The Sky Below

Abstract

Phantoms mimicking the specific mechanical and acoustic properties of human tissues are essential in the development and evaluation of novel ultrasound methods. In this work, various ultrasound phantoms are proposed to be used in the development of ultrasound methods to investigate the arterial walls longitudinal movements influence on the *vasa vasorum* circulation.

The longitudinal movement of arteries has been shown *in vivio*. It has been measured to be of the same magnitude as the diameter change of the arteries. Ultrasound phantoms simulating the arterial longitudinal movement has recently been made using Polyvinyl alcohol (PVA). However, these phantoms suffered from having low temporal stability and easy degradation.

This master's thesis investigates several tissues mimicking materials and describes the design and fabrication of ultrasound phantom models that simulate the *vasa vasorum* (the vessels of the vessel) and the longitudinal movement of the arterial wall. The mechanical properties of phantom materials were evaluated with a mechanical test instrument and the speed of sound was measured using a method based on the time of flight, and the attenuation was also measured. We showed that copolymer-in-oil, as well as ballistic gel, are excellent alternatives for vessel phantom fabrication. The Young's modulus for copolymer in oil and ballistic gel was measured to be 37 and 82 kPa, respectively. The attenuation coefficients were 0.83 and 0.40 dB/MHz/cm, respectively. The ultrasound speed ranged from 1433–1458 m/s.

The results suggest that the best alternative is to use the commercially available styrene-ethylene/butylene-styrene (SEBS) block copolymer in mineral oil, and the clear synthetic ballistics gelatin of 10%. A walled and multi-layered vessel phantom in a cylindrical geometry and with decreasing diameter was designed and fabricated. The longitudinal and radial movements were generated by the use of pulsatile flow produced from a gear pump. The longitudinal movement was measured to 0.2 mm and the radial movement to 0.8 mm.

Sammanfattning

Fantomer är viktiga för att utveckla och utvärderar nya ultraljudsmetoder. Fantomer kan även användas för att öka förståelsen för hur människokroppen fungerar. Det är nödvändigt att skapa fantomer med specifika mekaniska och akustiska egenskaper så att de kan simulera mänsklig vävnad. Ett exampel på fenomen som man vill veta mer om är den longitudinella rörelsen hos artärer. I det här projektet föreslås olika ultraljudfantomer som kan användas i utvecklingen av ultraljudsmetoder för att studera påverkan av artärväggens longitudinella rörelse på vasa-vasorumcirkulationen.

Den longitudinella rörelsen av artärer har visats *in vivo*. Den rörelsen har visat sig att vara i samma storleksordning som artärernas radiella rörelse. Ultraljudfantomer som simulerar den arteriella longitudinella rörelsen har tillverkats av polyvinylalkohol (PVA), men, dessa fantomer har låg temporal stabilitet.

I detta arbete har flera vävnadsliknande material undersökes. Dessa material har använts för att tillverka fantomer som efterlikanar artärer med *vasa vasorum* som kan uppvisa den longitudinella rörelse. Såväl utformning som tillverkning och testning beskrivs. De mekaniska egenskaperna hos fantommaterial utvärderades med ett mekaniskt testinstrument och ljudhastighet uppmättes med en metod baserad på *time of flight* och även dämpningen uppmättes. Vi visade att sampolymer i olja såväl som ballistisk gel är utmärkta alternativ för tillverkningen av kärlliknande fantom . Youngs modul för sampolymer-i-olja och ballistisk gel mättes till 37 respektive 82 kPa, dämpningskoefficienten var 0,83 respektive 0,40 dB/MHz/cm och ultraljudshastigheten varierade från 1433-1458 m/s.

Resultaten tyder på att fantomerna kan tillverkas av den kommersiellt tillgängliga styren-eten/styren (SEBS) segmentsampolymeren i mineralolja, och den klara syntetisk ballistikgelatin av 10%. En flerskiktsfantom i en cylindrisk geometri och med minskande diameter konstruerades och tillverkades, och des radiella och dess radiella och längsgående röresle till följd av ett pulserande tryck och flöde alstrat av en väx-

elpump undersöktes. Den longitudinella rörelsen mättes till 0.2 mm och den radiella rörelsen till 0.8 mm.

Acknowledgments

This thesis is dedicated to my mother for her unwavering support and endless kindness. Time flies, but some things remain the same, and I am thankful for that.

I would like to express my gratitude to my supervisor Magnus Cinthio, and co-supervisors Maria Evertsson and Sandra Sjöstrand. We have shared many things over the last few months, have had many ideas, some excellent, some merely good, and the rest forgotten. But personally, I will never forget my time here, and I hope our friendship will last through the years.

My sincere gratitude is also dedicated to Axel Tojo, Tobias Erlöv, John Albinsson, Désirée Jarebrant, Martin Bengtsson and Tomas Jansson from the Department of Biomedical Engineering, LTH, for their kindness and help throughout this work

Finally, I would also like to express my deepest gratitude to my family, especially my wife; the love of my life and the rock of our family, Hima. Thank you for providing me with unfailing support and continuous encouragement throughout my years of study and through the process of researching and writing this thesis. This accomplishment would not have been possible without you.

Thank you.

Benjamin Meirza

Contents

Chapter 1
Introduction

1.1 Background

Cardiovascular diseases (CVDs) killed 17.7 million people in 2015 and the World Health Organization estimates 23.3 million people will die from CVD in 2030 [1]. Furthermore, circulatory dysfunction represents the leading cause of the intensive care unit cost, admission and mortality. There has been great progress in treatment methods of CVD within interventional cardiology, and modification of frequently common risk factors such as hypertension, diabetes, dyslipidemia and atherosclerosis. However, CVD still remains the leading cause of death in the western world [2, 3, 4, 5, 6]. In Sweden, CVD is coupled with almost 28 000 heart attacks every year; in fact, it is the most common cause of death [7]. Given these points, the challenge is to develop methods for early detection of CVD, which can further improve the outcome of clinical treatments [8].

Understanding the hemodynamics of the blood vessels requires better knowledge of the complex cardiovascular system as well as the properties of the blood vessels [9]. During the cardiac cycle, the common carotid artery experiences a radial movement as well as a longitudinal movement [10]. The longitudinal and the radial wall movements of arteries have been shown *in vivo* [11]. The longitudinal movement has been measured to be in the same magnitude as the radial movement of the arteries [12]. The underlying mechanism of this movement and its function are yet not fully understood [13]. One function of this movement could be related to blood circulation in *vasa vasorum*. The *vasa vasorum* is a network of small blood vessels that play a nutritive role in the walls of large arteries [14, 15].

Recent studies have found a potential connection between the reduction in the longitudinal movement of the common carotid artery, in which *vasa vasorum* is found, and risk factors for CVD [16, 17]. Furthermore, there are evidences suggesting connections between some specific cardiovascular diseases and changes in *vasa vasorum*

morphology and hemodynamics [18, 14]. In particular, it seems that the *vasa vasorum* has a central role in the physiopathology of the aortic dissection, intramural hematoma and penetrating ulcer, which are three critical aortic syndrome entities [19].

Despite the attention that the *vasa vasorum* has been given and the potential pathophysiological significance of altered blood flow through *vasa vasorum* relatively little is known about its hemodynamics [15].

To obtain a better understanding of the possible effect of the longitudinal movement of the common carotid artery and the *vasa vasorum*, we need to develop a super resolution ultrasound method that can study the longitudinal movement of the arterial wall and the blood circulation in the *vasa vasorum* network simultaneously. Ultrasound phantoms are made of tissue mimicking materials which emulate important properties of human tissues. In addition, ultrasound phantoms are essential tools used in the development and characterization of imaging algorithms and techniques [20].

To be able to develop such a method, an ultrasound phantom with known geometry and composition is needed. The obtained knowledge can provide information that might be used for early detection of CVD [20].

1.2 The aim

The aim of this project was to design and fabricate a suitable phantom model of an artery and the *vasa vasorum* to be used to develop ultrasound methods for studying the possible effect of arterial longitudinal movement on blood regulation within the *vasa vasorum*. To do this, different phantoms were developed with various complexity levels, where an artery and its *vasa vasorum* was designed and fabricated using different tissue mimicking substitutes. The ideal phantom should act in the same manner as the human artery and its *vasa vasorum*. Furthermore, the mechanical and acoustical properties should be similar to that for human vessels and surrounding tissues.

1.3 Objective

1. Test different tissue substitutes for ultrasound imaging and suggest a suitable material.

2. Design and fabricate a phantom consisting of a model of arteries and *vasa vasorum*.

3. Suggest future work and application.

1.4 Approach and methodology

1. Conduct a literature study of the anatomy of the artery and *vasa vasorum*, the longitudinal movement of arteries and tissue substitutes for ultrasound imaging.
2. Design and fabricate molds using various techniques.
3. Create phantom prototypes.
4. Evaluate the properties and functionality of the phantoms.

Chapter 2
Theory

2.1 Anatomy and functionality of the arteries

Arteries are blood vessels responsible of carrying oxygenated blood from the left ventricle of the heart out to the body [21]. Three cell types play an important role in the biomechanics of the normal arterial wall: fibroblasts, smooth muscle and endothelial cells. Each of these cell types is quick to respond to any variations in their mechanical environment. Furthermore, it is well known that the arteries creep and stress relax, and also show hysteresis upon cyclic loading [22].

The arterial walls consist of three primary layers, in which *vasa vasorum* is found (Figure 2.1).

Tunica Adventitia : Consists of connective tissue, axially oriented collagen and elastic fibers. Adventitia is the "strong" cover layer of arteries, thereby plays an important role as a structural support for some vessels.

Tunica Media : The middle and thickest layer, consists of smooth muscle cells embedded in a plexus of elastin.

Tunica Intima : The inner layer consists of a monolayer of endothelial cells and an elastic membrane. The inner layer of the arteries and veins is referred as endothelium and is very active biologically.

vasa vasorum: Have few layers of smooth muscles, innervated by sympathetic fibres and is the vasculature [24] .

The diameter of the aorta is $10 - 20$ mm and it gets more narrow distally. The thickness of the tunica intima and tunica media combined is approximately 0.5 mm for a healthy 20 years old human. This thickness is not constant throughout the

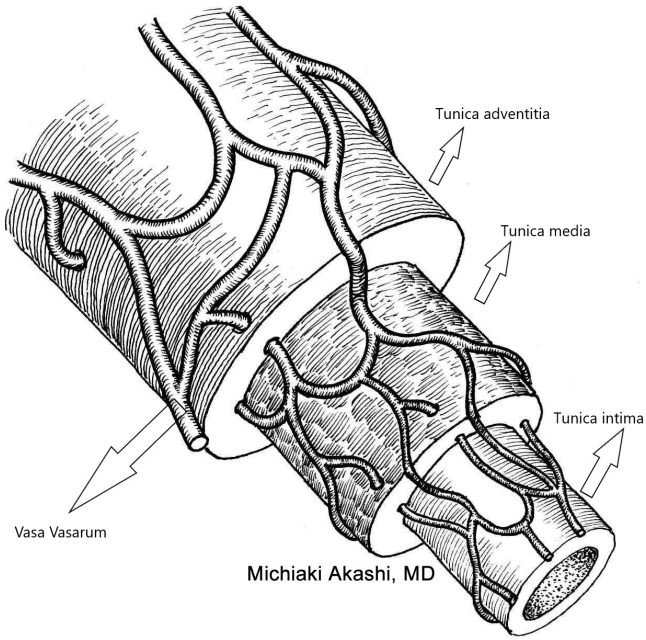

Figure 2.1: Terminology used to describe anatomy. The arterial walls layers: Tunica intima,Tunica media and Tunica adventitia. Used with permission from Clinical Anatomy Associates, Inc [23].

human live; it changes and becomes thicker. At 70 years old the thickness is almost 0.9 mm [25] .

2.2 Longitudinal movement

During the cardiac cycle, the arterial wall experiences a radial movement as well as a longitudinal movement. Figure 2.2 illustrates the radial and longitudinal movements of the arteries. The radial movement of the common carotid artery has been extensively investigated during the last 30 years compared to the longitudinal movement [10]. This is probably due to the difficulty in implementing measurements of the longitudinal movement and the lack of an adequate measuring technique [26]. However, recently, by using modern ultrasound technique it has been possible to measure and describe the longitudinal movement and the intramural shearing of the arterial

Figure 2.2: Illustration of the radial and longitudinal movements.

wall [10].

Studies found that the intima-media layer of the arterial wall shows the largest longitudinal movement. This movement was measured to be around $0.1 - 1$ mm in the common carotid artery, which is of the same magnitude as the radial movement. Additionally, a smaller magnitude of the movement with the same basic pattern has been found in the adventitial layer of the arterial wall. Moreover, different people show a different pattern of the longitudinal movement [27]. In general, the proximal and more elastic arteries show larger longitudinal movement than distal arteries [10].

The longitudinal movement of the common carotid artery of a healthy human is shown to be distinctly multiphasic and bidirectional, with a distinct ante-grade movement in early systole and a retrograde movement later in systole. In diastole and before the wall gradually returns to its original position a second ante-grade longitudinal movement is taking place [10].

Recently, an ultrasound phantom exhibiting the longitudinal movement of the common carotid artery was designed and fabricated from polyvinyl alcohol. When subjecting the phantom to a pulsatile pressure, a 220 µm displacement in the longitudinal direction was demonstrated [28].

2.3 Vasa vasorum: Anatomy and functionality

The term *vasa vasorum* comes from Latin and means "the vessel of the vessels". The function of the *vasa vasorum* is to provide an important blood supply and nourishment to arteries and veins [17].

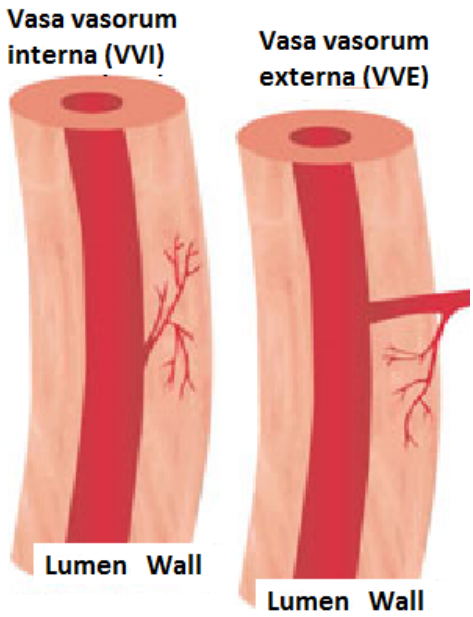

Figure 2.3: Two types of *vasa vasorum*, *vasa vasorum* externa and *vasa vasorum* interna [29].

Vasa vasorum consists of small blood vessels that penetrate the arterial wall and can be categorized depending on the location it penetrates the vascular wall. There are two types of *vasa vasorum* (Figure 2.3) [21].

- *vasa vasorum* externa penetrates the vascular wall from the abluminal surface which is the surface away from the lumen
- *vasa vasorum* interna that enters the vascular wall from the luminal surfaces which is the surface adjacent to the lumen

The structure of *vasa vasorum* varies with the function, location and size of the vessel. In normal arteries, vasa vasorum branches from the adventitial layer of large arteries into the media to actively regulate blood flow to the arterial wall. In addition, not all vessels have *vasa vasorum*, smaller vessels, with a wall thickness less than 25 cell layers and vessels less than 0.5 mm lumen diameter [21] lack *vasa vasorum*. Furthermore, the arterial vasa have a straighter course and less numerous, branches and have a smaller lumen than the veins [30].

2.4 The dynamics of vasa vasorum

The intramural pressure gradient within the arterial wall is in agreement with Lame's law 2.1 and can result in compression of the *vasa vasorum*. Moreover, the anatomic location and the branching shape of the *vasa vasorum* externa has an important consequence, and that is that the blood flow through the *vasa vasorum* cannot go on far into the media as a consequence of the compressive force (P_w) within the arterial wall, at location R. This is mathematically described by Lamé's Law 2.1.

$$Lam'sLaw : \frac{P_w\,(R)}{P_\ell} = a^2[\frac{1-(b/R)^2}{b^2-a^2}] \tag{2.1}$$

Where P_ℓ is the pressure in arterial lumen, a is the radius of the arterial lumen, b is the radius of the outer adventitia, and R is the radial distance within the arterial wall.

Diffusion of blood solutes must be from the lumen towards the adventitia, which can be explained by the pressure difference between the arterial lumen and the extravascular tissue. This can be described by Darcy's Law 2.2. Thus only via *vasa vasorum* or any lymphatics in the wall can solute leave the vessels wall.

$$Darcy'sLaw : \frac{f_\ell}{f_v v} \propto (\frac{Area_\ell}{Area_v v})\,(\frac{R+T}{R})^3 \tag{2.2}$$

Where f and $f_v v$ are the fluxes of blood from the arterial lumen and into the venous *vasa vasorum* respectively. $Area$ is the coronary arterial endothelial surface area across which solute flux occurs and $Area_v v$ being the area of the vasa endothelial surface within the wall at distance R within the wall. T is the distance from the endothelium towards the outer surface of the adventitia (i.e., $R-a$). The resistance of the *vasa vasorum* is high due to its considerably small radius relative the vessel lumen, in particular in larger arteries as the aorta. The pressure drop (P_i) along the *vasa vasorum* is described by Poiseuille's Law 2.3.

$$Poiseuille'sLaw : \Delta p_i \propto \frac{L_i}{r_i^4} \tag{2.3}$$

Where: pi is pressure in lumen of *vasa vasorum* at distance L from the origin of the *vasa vasorum*. ri is the radius of the 'proximal' *vasa vasorum* lumen and Li is the distance along the *vasa vasorum* to the point-of-interest within the wall. The velocity of blood flow is inversely proportional to the total cross sectional-area of the blood vessels. As described in equation 2.4.

$$V = \frac{Q}{A} \tag{2.4}$$

where V is the velocity (cm/s), Q is blood flow (ml/s) and A is cross sectional area (cm^2). Additionally, the blood flow velocity in the middle of the vessels is faster than that at the vessel wall, under the laminar characteristics of the blood flow. Blood velocity for two types of blood vessels and how it is related to the cross-sectional area in the body is shown in table 2.1.

Type of blood vessels	Total cross-section area (cm^2)	Blood velocity in (cm/s)
Aorta	3–5	40
Capillaries	4500–6000	0.03

Table 2.1: relationship between blood velocity and the total cross-sectional area [31].

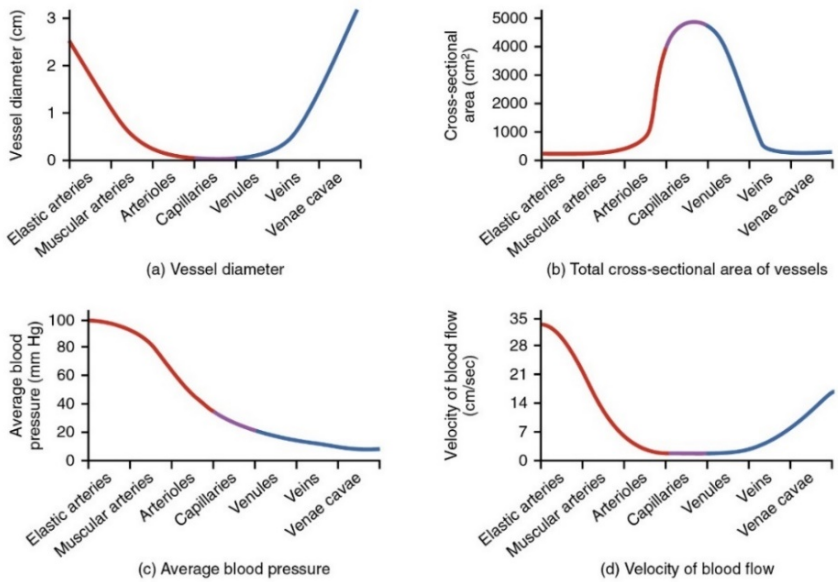

Figure 2.4: Relationships among Vessels. Various relationships among blood vessels (a) vessel diameter, (b) total cross-sectional area, (c) average blood pressure and (d) velocity of blood flow [31].

2.5 Ultrasound theory

Ultrasound is a sound wave of a frequency higher than 20 kHz. For medical imaging applications, frequencies of 2 to 15 MHz are used. Ultrasound propagates as a

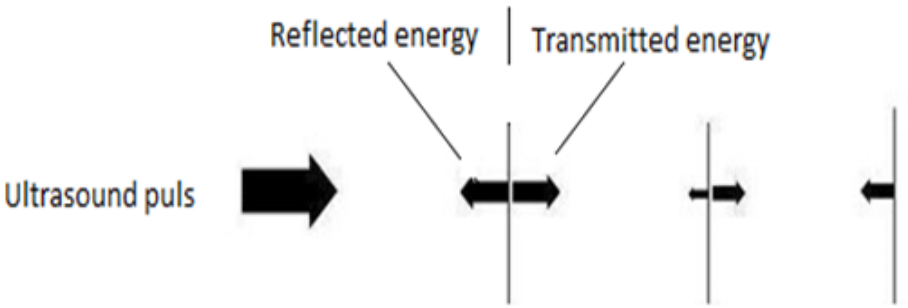

Figure 2.5: An ultrasound wave is sent by the transducer, some of the waves is reflected by a boundary between two medium with different acoustic impedance and the rest is transmitted, the reflected wave which is also called echo returns to the transducer.

longitudinal wave, meaning that the tissue molecules are moving forward and backward in the same direction as the wave propagation. Ultrasound may oscillate the medium transversely as well; such a wave is called a transverse or shear wave. Longitudinal waves are of higher relevance in soft tissue, while shear waves propagate in hard tissues such as bone and tooth.

In medical applications, ultrasound is produced by using piezoelectric crystals that vibrate at extremely high frequencies, when an electrical voltage is applied, an effect called piezoelectric effect is produced.

The speed of sound, c, of a longitudinal wave is related to the wavelength, λ, and the frequency, f, by equation 2.5

$$c = \lambda \times f \tag{2.5}$$

Ultrasound interactions are determined by the acoustic properties of tissue. As an ultrasound wave propagates through the body tissue, several interactions occur, such as reflection, refraction, scattering and absorption. At each tissue interface, the wave will be reflected. If the incident beam is perpendicular to the boundary, a part of the energy will be reflected back to the transducer, whereas the rest, will continue in the initial direction (Figure 2.5).

Reflection provides the basis for ultrasound imaging techniques, when an ultrasound wave strikes a boundary between two media of different acoustic impedance,

some of the waves energy continue into the second medium, and some is reflected back as an echo. The amount of the transmitted and thereby the reflected energy primarily depends on the acoustic impedance, Z. However, factors such as the angle of incidence, the width of the tissue structure and the angle of the tissue boundary are important. The acoustic impedance Z can be calculated as in equation 2.6, where ρ is the material density in which the sound wave is propagating.

$$Z = \rho \times c \tag{2.6}$$

Scattering is a reflection from small or rough targets. When ultrasound interacts with a small object or rough surfaces, the reflected waves are redirected in several directions. The size of the target affects the uniformity of the scattering and also determines the directions of the scattering. A target of a size smaller than a wavelength will reflect the incident wave uniformly and in all directions.

Absorption is the conversion of kinetic energy to heat from the propagating ultrasound wave. This continuous process results in a reduction in echo amplitude with depth. Furthermore, absorption is important for two main reasons, one is that heating can affect tissues, thus, it is a safety limitation, the second reason is the attenuation which is mainly due to absorption and is the limiting factor for how far in the tissue the ultrasound wave can propagate, i.e. the penetration depth of the beam.

The depth needed to reach human anatomy determine the ultrasound frequencies used for medical imaging techniques, which range, as stated before, from 2 to 15 MHz for most applications. Within this range the lower frequencies are used to look at deeper body structure and the higher frequencies for superficial structures. The reason behind this is that the high-frequency ultrasound waves are more attenuated than lower frequency waves for a given distance, as described in equation 2.10, [32, 33]

2.6 Speed of sound

The speed at which an ultrasound wave propagates is determined by the mechanical properties of the medium. For soft tissues and liquids, the speed of sound, c, is controlled by the compressibility, K, and the density, ρ. Mathematically this is expressed in the equation 2.6.

c = $\sqrt{}$(K/ρ)(2.7)

The sound velocities through different tissues are shown in table 2.2. Notice that the sound velocity is highest through bone which is the tissue with the highest density [32, 33].

Medium	Velocity (m/s)
Water	1480
Soft tissue	1540
Kidney	1560
Blood	1570
Muscle	1580
Bone	4080

Table 2.2: Sound velocities through different tissues [32, 33].

2.7 Attenuation

Attenuation of ultrasound occurs when it is propagating through a medium. The reason behind this phenomenon is that the energy is absorbed by the tissue in form of heat and scattering. Attenuation of ultrasound in human tissue is approximately 1dB/cm/MHz, see table 2.3 for the attenuation coefficient of different types of human tissues.

Medium	Attenuation Coefficient (dB/cm at 1MHz)
Water	0.002
Blood	0.18
Fat	0.63
Liver	0.5-0.94
Muscle	1.3-3.3
Bone	5

Table 2.3: : Attenuation coefficient for different human tissues[32, 33].

The reduction in acoustic pressure amplitude of the incident wave in a tissue is characterized by its attenuation coefficient. The acoustic attenuation coefficient, α (dB/cm at 1MHz), can be defined as the sum of the attenuation due to absorption, α_a, and the attenuation due to scattering, α_s

$$\alpha = \alpha_a + \alpha_s \tag{2.8}$$

The overall ultrasound attenuation is characterized by the exponential decrease of the intensity amplitude, I, during propagation through tissue, equation 2.9,

$$I = I_0 \times e^{-\alpha x} \tag{2.9}$$

where: I_0 is the initial intensity, x is the ultrasound propagation distance and α is the attenuation coefficient.

The attenuation coefficient is affected by the frequency of the ultrasound wave. The higher the frequency, f, the larger is the amount of attenuated energy by the medium. The attenuation coefficient can be described via a power law:

$$\alpha(f) = \alpha \times f^n \tag{2.10}$$

where: α is the attenuation coefficient (nepers/cm/MHz), f is the frequency (in MHz) and n is a material-dependent parameter. [32, 33].

2.8 Basic viscoelasticity

A material can respond to physical stress in three ways. It can apply the stress it senses directly onto the forces that hold the atoms or the molecules in place, as is the case in ceramic materials and simple crystalline including polymeric crystalline. This type of material response can be exemplified among biological activity as in when a muscle pulls on a bone. The material can also feed the energy into large semi-permanently (as viscoelastic materials) or irreversible (as plastic materials) shape deformation [34, 35].

The behavior of the material response to the stress is the summed responses of each bond within it, therefore, the more force applied on a piece of material the stronger the response. Hook described this phenomenon as ut tensio, sic vis, which means "as the extension, so the force" [36]. In other words, strain and stress are directly proportional to each other as described in equation 2.11.

$$Stress/strain = constant \tag{2.11}$$

In order to estimate the strain, measurements are performed on a piece of material and the change in the length of the sample is obtained. The increase in the length can then be described as Cauchy strain, which is the increase in the sample length per unit starting length [33]. The Cauchy strain has no units, and can mathematically be written as in equation 2.12.

$$Strain = \frac{(length(after) - length(before))}{(length(before))} \tag{2.12}$$

The force acting on each individual bond depends on the number of bonds that share the load, thus the stress expressed as force F divided by the cross-sectional area A of the sample on which the force is acting.

$$Stress = \frac{F}{A} \tag{2.13}$$

The constant in equation 2.11 is known as Young's modulus, E . Equation 2.11 then becomes

$$Stress/strain = E \tag{2.14}$$

Typical values of Young's Young's modulus of human tissues and tissue mimicking materials are given in tables 2.4, and 2.5, respectively.

Table 2.4: Young's Modulus [kPa] for different human tissues [32, 33].

Tissue	Young's Modulus (kPa)
Brain	1-4
Breast	1-3
Cardiac	10-15
Diseased Liver	6-25
Liver	8-12
Muscle	20-20
Marrow	0.5-1.5

Table 2.5: Young's Modulus [kPa] for different tissues mimicking materials [32, 33].

Material	Young's Modulus [kPa]
Silicone rubber	500-5000
PVA Cryogel tissue mimic	35-500
Agar/ Gelatine tissue mimic	10-70

[32, 33].

2.9 Rheological models for viscoelastic materials

A viscoelastic material behaves mechanically a bit like a fluid and a bit like a solid. By considering combinations of the linear elastic spring and the linear viscous dashpot, rheological models of a viscoelastic material can be built up. The constitutive

mathematical equation for materials that respond as a linear elastic spring is:

$$\varepsilon_e = \frac{1}{E}\sigma \tag{2.15}$$

Where , E is Young's modulus, and $\sigma$is the stress.

The response of materials that react like viscous dash-pot can be described mathematically as in equation 2.16

$$\dot{\varepsilon_v} = \frac{1}{\eta}\sigma \tag{2.16}$$

in which $\dot{\varepsilon_v}$ is the strain velocity and η is the viscosity of the material. Many fluids typically respond in this way; straining is usually faster when the stress is large. The linear elastic spring and the linear viscous dash-pot are illustrated in Figure 2.6.

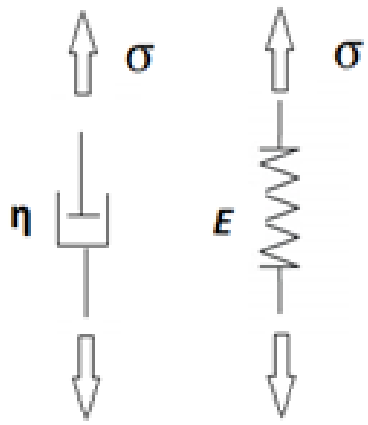

Figure 2.6: Dash-pot (left) and spring model (right) for viscoelastic building elements for rheological model.

By series and/or parallel coupling of both elements in Figure 2.6 , more or less complex material models can be represented

2.10 The Maxwell model

Models in which a spring and dash-pot are in series are called Maxwell-materials, see Figure 2.7

Since the two elements are in series, the stress experienced by the spring is the same experienced by the dash-pot. The total strain ε_t for Maxwell material is

$$\varepsilon_t = \varepsilon_e + \varepsilon_v \tag{2.17}$$

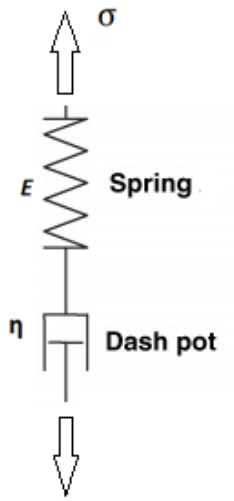

Figure 2.7: The Maxwell Model.

By differentiating the equations: 2.15 and 2.17 , and than putting in the equation 2.15, and equation 2.16 into equation 2.17 one gets

$$\sigma + \frac{\eta}{E}\sigma^{\cdot} = \eta\varepsilon^{\cdot} \tag{2.18}$$

This constitutive equation shows the relation between the stress and the strain in the material.

2.11 The Kelvin (Voigt) model

The Kelvin model consists of a spring and dash-pot in parallel, see Figure 2.8

Since elements are in parallel the strain experienced by each element is the same. This time,

$$\varepsilon_e = \tfrac{1}{E}\sigma_1 \tag{2.19}$$

$$\varepsilon_v^{\cdot} = \tfrac{1}{\eta}\sigma_2 \tag{2.20}$$

$$\sigma = \sigma_1 + \sigma_2 \tag{2.21}$$

Eliminating σ_1 and σ_2 leaves the constitutive equation

$$\sigma = E_o\varepsilon_e + \eta_o\varepsilon^{\cdot} \tag{2.22}$$

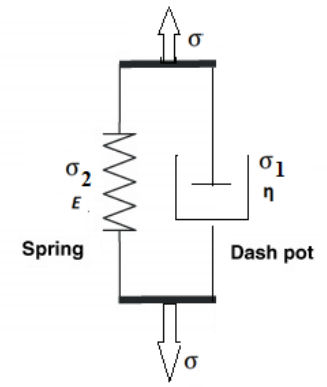

Figure 2.8: The Kelvin(Voigt) Model.

2.12 Soft tissue mimicking materials for ultrasound imaging

Since 1960, ultrasound phantoms have been used in characterization and calibration of various ultrasound systems.

As mentioned in chapter 2.5, when an ultrasound wave passes through tissues with different acoustic tissue properties such as the speed of sound, acoustic impedance, attenuation and absorption, it interacts in various ways. These interactions affect the ultrasound pulse-echo signals and are necessary to form an ultrasound image. Furthermore, the acoustic properties of tissues are not constant either among people or within the same human, and the sound velocity and attenuation also vary depending on the temperature. The knowledge of these parameters and how they vary depending on the frequency, pathology, temperature, age and amplitude is essential for us to understand in order to make the most efficient ultrasonic imaging techniques [20].

The *ideal* tissue mimicking material for constructing ultrasound phantoms should have the same ranges of attenuation, scattering coefficients and the sound velocity as tissues. These parameters should be controllable in the material preparation process, stable within the range of room temperature and with time as well as ease of storage [37].

To date, a wide range of soft tissue mimicking material have been employed in ultra sound phantom fabrication [20]. A multitude of these and their respective acoustic properties are listed in table 2.6.

Material	Velocity (m/s)	Attenuation (dB/cm/MHz)	Advantage	Disadvantage
Agarose-based	$1498 - 1600$	$0.04 - 1.40$	Well-documented, frequently used and easy to fabricate	Delicate structure
Gelatin based	$1520 - 1650$	$0.12 - 1.5$	Stable in room temperature	Unstable with temperature variations, and scatter uniformity
Magnesium silicate-based	$1458 - 1520$	0.85	Stable as long as the temperature is between 0-100 Celsius degree, resistance to microbial invasion	Incapability of sculpture or mould
Oil-based	$1480 - 1580$	$0.4 - 1.8$	The speed of sound and the attenuation increases linearly with the propylene glycol content. Immune to bacterial invasion	Low attenuation and high speed of sound for ethylene glycol-based phantoms
Open cell foam based	1540	0.46	Can be used to manufacture inhomogeneous phantoms	The attenuation is affected by temperature variation
Polyarcrylimide Gel-based	1540	0.7 dB/cm MH	The speed of sound and the impedance are similar to those for soft tissue	Low attenuation, toxic
Polyuerethane	1468	0.13	The attenuation increases linearly with frequency and temperature	Complexity of manufacture
Tofu	1059	0.75	Inexpensive	Lower nonlinear parameter than soft tissue. Properties cannot be changed as desired

Table 2.6: A list of various tissue mimicking material and their acoustic properties, advantages and disadvantages [20, 38, 39, 40, 41, 42].

2.13 Styrene-ethylene/butylene-styrene (SEBS) block copolymer in mineral oil

SEBS, was announced in 1972. At first it was mainly used in footwear, packaging or adhesive industries [43]. The microstructure of SEBS, see Figure 2.9, consists of a molecular structured elastomer with two phases; a styrene rigid structure and a rubbery ethylene-butylene structure [44]. In order to soften the ethylene butylene phase of the SEBS copolymer, various plasticizer can be used such as mineral oil. The use of the palsticizer increases the processability of SEBS as well as modifies the SEBS in mineral oil properties [45].

SEBS gels are thermoreversible and oil-based materials and do not dehydrate. Furthermore, SEBS is immune to bacterial invasion and therefore present good temporal stability. These copolymers in mineral oil are proven to have acoustic and mechanical properties similar to those for human tissue and have therefore been suggested as tissue mimicking materials [40]. According to Cabrelli et al. [40] it is possible to control the acoustic parameters of copolymer-in-oil gels such as SEBS. By changing the concentration of SEBS copolymer in mineral oil, the mechanical and acoustic properties are changed. The same effect occurs if other substances are added such as low-density polyethylene [46].

Moreover, a blend of white-silicone rubber and SEBS gel has been reported as a tissue mimicking material, by adding white-silicone to SEBS gels, the speed of sound is decreased while the acoustic attenuation is increased [47].

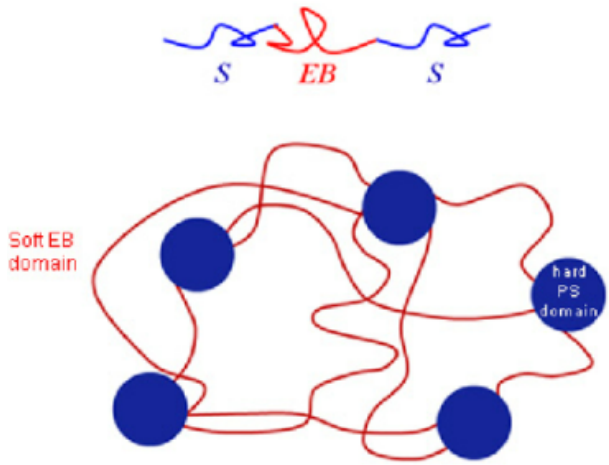

Figure 2.9: The microstructure of SEBS copolymer. A styrene rigid structure and a rubbery ethylene-butylene structure [44].

2.14 Clear ballistics gel and Polydimethylsiloxane as tissue mimicking materials

Ballistic gel is a thermoplastic gel that is versatile, odorless, reusable, inexpensive and does not decay and it is usually used as an analogue to human flesh for firing training and other military evaluations. Ballistic gel is also well established and used as ultrasound phantom materials [48, 49, 50].

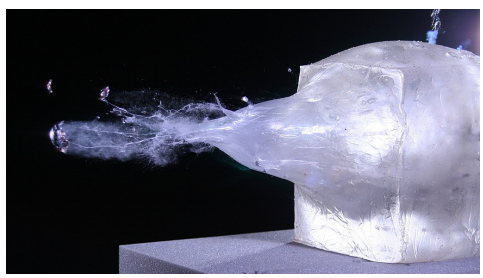

Figure 2.10: Photo of synthetic ballistic gelatin showing terminal fragmentation of a .243 projectile [51].

Polydimethylsiloxane (PDMS) has also been used as vessel mimicking material and the reported speed of sound was 1020±20 m/s [52]. according to Tsou et al.

[53], the change in the ratio of the curing agent to polymer base has an effect on the speed of sound. A ratio of (1:5) could result in a speed of sound of 1119.1 m/s. Their findings are summarized in table 2.7.

Ratio of Curing agent: Polymer base	5 : 1	7 : 1	10 : 1
Speed of Sound (m/s)	1119.1	1089.1	1076.5

Table 2.7: Speed of sound for polydimethylsiloxane reported by [54].

2.15 Towards realistic blood vessel phantoms

A realistic blood vessel ultrasound phantom for ultrasound measurements is essential for advanced experimental biomedical research [55]. To date, several blood flow vessel phantoms have been published [56]. However, existing blood vessel phantoms suffer from not having the optimal acoustic, mechanical, optical and temporal properties simultaneously [55].

As mentioned in section 2.1, a blood vessel is constituted of soft tissue, collagen, elastin, smooth muscle, and so on. It behaves as a viscoelastic material. In addition, the cardiac and respiratory cycle causes changes in the stress that these vessels experience. Therefore, in order to fabricate a vessel phantom that behaves in the same way as a living vessel during pulsatile flow, it is important to represent the dynamic viscoelasticity of a living blood vessel [41].

Several types of materials have been suggested to mimic the blood vessel wall including latex, C-flex and glass [57, 55].However, these phantom materials tend to have very high attenuation coefficient [58] and to overcome this problem, researchers have used other methods, such as, excised human vessels [59, 60]. However, due to ethical issues, this method is not ideal. Another approach to the development of realistic blood vessel phantoms it to develop wall-less vessel phantoms. These phantoms overcome the problem of high attenuation, and enable different geometries and shapes were possible compared to the conventionally used materials. Yet, these phantoms could not be used for investigating different physiological phenomena related to the vessel wall itself [60].

The *ideal* solution lies in the development of methods that can can provide materials with tailored acoustic and mechanical properties.

Chapter 3
Materials and Methods

3.1 Selecting tissue mimicking material

Several tissue-mimicking materials have been investigated in this project, such as Polyvinyl alcohol (PVA), Polydimethylsiloxane (PDMS), Styrene-Ethylene/Butylene-Styrene (SEBS) in mineral oil and the oil based Ballistic gelatin (Clear Ballistics). To investigate whether the tissue-mimicking material was suitable to be used as a phantom material for the *vasa vasorum* phantom an initial test was performed. The test included designing and manufacturing a simple wall-less vessel phantoms to determine if the material used was easy to separate from the mold and also to check if the vessel like channels in the phantoms were reasonably visible for the ultrasound.

3.2 Gel preparation

The SEBS gel was prepared by mixing SEBS (Karaton G 1650M, Kraton Polymers) in mineral oil (Paraffin olja, TRIKEM VET, Malmö, Sweden) at room temperature. The mixture was then placed in the oven and heated to 130° C until a homogeneous clear solution was obtained. In order to have complete homogenization and polymerization, the mixture had to be stirred occasionally. Following that, the mixture was left to cool in room temperature while kept in molds with known dimensions until solidification. Three sets of phantoms were manufactured using different concentrations of SEBS, for acoustic characterization.

Clear synthetic ballistics gelatin of 10% was prepared in the same way. One phantom was prepared using PDMS of in the ratio of 1:5 (curing agent to polymer). The mixture was placed in a mold and then degassed in a vacuum chamber for 30 minutes. Thereafter heated in the oven at 75° C for 1 h to complete the curing process. This phantom was manufactured to determine if glass capillary (164 µm in diameter)

could be withdrawn in order to leave a vessel like channel behind.

3.3 Glass beads

Glass beads with a mean diameter of 93 µm (Potters Industries, Valley Forge, PA, USA) were used. 4, 5 or 7 g glass beads per liter were added to the chosen material for each part of the phantom. This provided strong and distinct echoes in the ultrasound images needed for the movement tracking algorithm

3.4 Blood vessel phantoms with vasa vasorum exhibiting the longitudinal movement

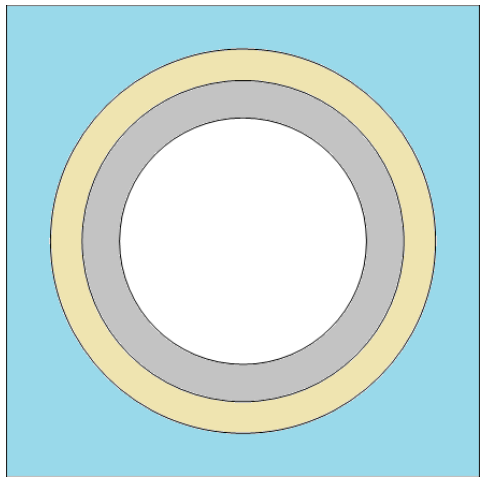

Figure 3.1: A schematic cross-sectional representation of the vessel; the intima-media complex (gray), connective tissue (yellow), the adventitia and the surrounding tissue (blue).

The *ideal* phantom would consist of three different layers, see Figure 3.1. An inner layer representing the intima-media complex and its *vasa vasorum*, while the outer and covering part mimicking the adventitia and the surrounding tissue. These two layers are needed to be able to glide against each other and at the same time be connected. To do this the middle part has to be the most elastic part and made of a fluid-like material. The longitudinal movement of the intima-media complex is large compared to the movement of the adventitial layer, and this was the main reason

behind the material chosen for each part. Furthermore, the phantom is needed to be manufactured with certain geometry, of suitable phantom materials and in an optimal way for ultrasound imaging technique to detect the longitudinal movement and the hemodynamics of the *vasa vasorum*. Additionally, as discussed in 2.15, the phantom is needed to have relatively high resistance to mechanical stress to best mimic the artery and its *vasa vasorum*.

3.5 Molds

3.5.1 3D printed molds

The designing and fabrication of different 3D models include three steps: first different 3D models were designed by using the CAD programs Fusion 360, Autodesk, San Rafael, CA, USA. Second, the created drawings of the models were converted into instruction for 3D printing, using a software called Cura, Ultimaker B. V., Geldemalsen, Netherlands. In the final step of the model fabrication, the 3D printer that was used made the models by applying melted Polylactic acid (PLA), layer by layer from a nozzle.

3.5.2 Handmade molds

For the fabrication of a phantom with a simple shape and geometry, aluminum foil and cardboards were used to manufacture different cubic molds.

The melted phantom material was poured into the molds while hot. Therefore, the materials of which phantom molds were fabricated have to be chosen so that their melting point, as well as the glass transition temperature, are suitable.

3.6 Elasticity measurement

A tensile test machine, MTS Systems AB, Minnesota, USA, was used to measure the viscoelasticity of different phantom materials used in this project, see Figure 3.2. These tests include applying a displacement to a sample and monitoring how the force required to maintain the displacement decays over time.

Five samples of SEBS and five samples of the clear ballistic material were analyzed. The samples were fabricated by pouring the melted gels in cylindrical metallic molds with a diameter of 12 mm. The samples were then analyzed in randomized order. All specimens were loaded with a force equal to 0.5 N and thereafter compressed with at speed of 1 mm/s so that the length of each sample analyzed is compressed with 25% of its original and measured height. The samples were kept under pressure for 6

minutes. The tensile test machine delivered the output in *txt* which was then used in Matlab.

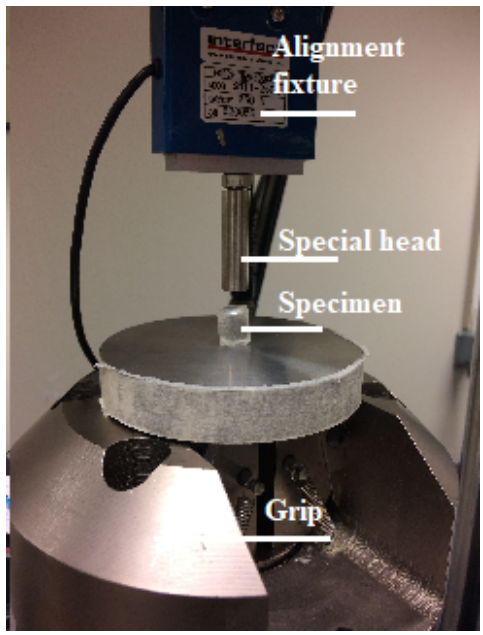

Figure 3.2: MST Universal Testing Machine used for testing the materials mechanical properties in this study.

Figure 3.3 shows the rheological model chosen to describe the phantom material. This model which is also called the standard linear viscoelastic model can be described with equation 3.1.

$$\sigma(t) = E_2\varepsilon_0 e^{\frac{-E_2 t}{\eta}} + E_1\varepsilon_0 \tag{3.1}$$

Where $\sigma(t)$ is the stress as a function of time, η is the viscosity and ε_0 is the initial strain. E_2 and E_1 are the elasticity values. A developed Matlab-script was used to produce a stress-time graph for each phantom material.

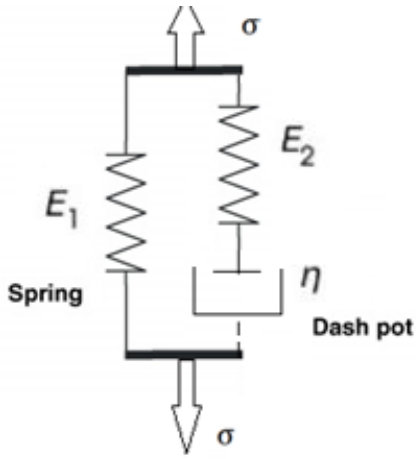

Figure 3.3: The chosen rheological model to represent the phantom material.

3.7 Measuring the speed of sound

Measuring the speed of sound within different tissue mimicking materials can be performed with reasonable levels of accuracy over the frequency range used for medical imaging.

The types of equipment used to measure the speed of sound, are shown in Figure 3.5.To have the best control over the dimensions, the solidified phantom material was kept in the mold, see Figure 3.5 c.

Five measurements were carried out for each phantom material. The transducer was placed in different positions and/or different distances from the phantom. Three phantoms with dimension of 2x4x3 cm and were made of 2% SEBS, 5% SEBS and 8% SEBS in mineral oil and a forth one of ballistic gel.

A method based on the time-of-flight was used. A short ultrasound pulse was emitted by a transducer. A part of the emitted pulse was reflected at each interface, see Figure 3.4. The reflected pulses were detected by the same transducer, which then transformed the sound pulses into electrical pulses. The detected pulses were displayed on the oscilloscope, from which the time difference, ΔT, between the front reflection signal $E1$ and the back reflection signal $E2$ was obtained. The data from the oscilloscope analyzed using a Matlab code (see Appendix). $E2$, see Figure 3.4 is the signal that was phase-reversed to be able to get the time difference between the signals. This information was put in the equation 3.2 to get the speed of sound.

$$c = \frac{2d}{\Delta t} \tag{3.2}$$

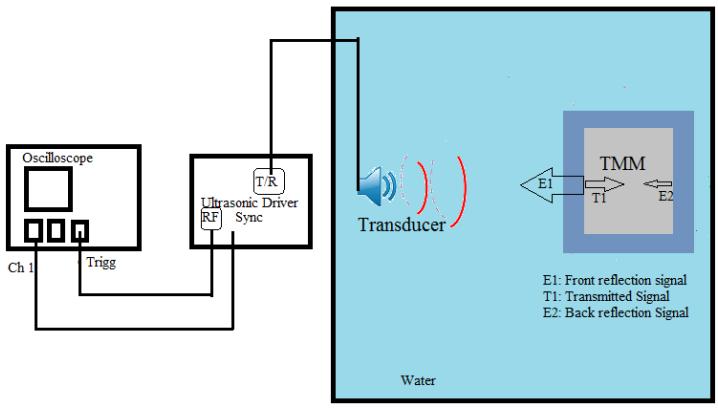

Figure 3.4: Scheme of setup used for measuring the speed of sound based on time of flight method.

Figure 3.5: The equipment used to measure the speed of sound, (a) the transducer and the mold in which the phantom material was kept, (b) the transducer, (c) the mold and the phantom material, (d) the water tank, The pulse generator and the oscilloscope.

3.8 Measuring the attenuation

The following equipment used for measuring the attenuation: A clinical ultrasound scanner (Philips Epiq 7), a hydrophone (0.5 mm in diameter, Precision Acoustics LTD), a broadband (1-6 MHz) clinical ultrasound transducer (X6-1 XMatrix, Philips), a filled water tank, and an oscilloscope (Tektronix TDS 360).

The phantoms were placed in the water tank in front of the transducer and in its far field. The hydrophone was placed close to the phantom facing the transducer.The ultrasound pulses that were transmitted through the phantom were recorded with the oscilloscope and transferred to a computer for analysis.

Six phantoms were made with the dimensions 1 x 2 x 1 cm; three made of SEBS and three made of ballistic gel. Two attenuation measurements were carried out for each phantom, once through 1 and another through 2 cm of sound penetration. The mean difference between these measurements (= 1 cm of sound penetration) in three phantoms was used to estimate the attenuation of each material. The attenuation was estimated in the frequency domain (FFT) using:

$$A = A_0 e^{-\alpha y} \tag{3.3}$$

Where A and A_0 are the amplitudes estimated in the frequency domain (FFT) measured after the ultrasound pulses penetrated the phantoms along the long and short axis separately, α is the attenuation in dB/cm/MHz and y is the pulse propagation distance.

3.9 Manufacturing of simple micro vessel phantoms

To create simple and wall-less vessel phantoms the following steps were taken:

Step 1: Gathering the following materials: heat protective gloves, foil paper, glass capillaries of various diameter, an oven and SEBS in mineral oil of a certain concentration or clear ballistic gel.

Step 2: The mold is prepared. A simple handmade cubic mold of aluminum foil and glass capillaries with different diameters $150, 175, 375$ µm are used, see Figure 3.6.

Step 3: The selected gel is cut into smaller pieces to decrease melting time.

Step 4: The gel is heated in the oven to 130° C. If the gel material contains bubbles, heat is continued in the oven until the bubbles disappear.

Step 5: The melted gel is poured into the mold and left to cool until solidification in rooms temperature.

Step 6: After solidification the glass capillaries are withdrawn carefully and a quality test is performed by investigating the phantom using ultrasound machine to check whether the vessel-like channels are seen by the ultrasound machine or not and also to check for the quality of the channels.

The phantom can be reused, buy cutting the phantom and reheated and then repeating steps $1 - 6$.

In order to have a fluid flow through the vessels, plastic tubes were needed for the connection to a standard lucer-lock syringe.

3.10 Creating thin film (2mm)

Using a mold created by a 3D printer, 2 mm thick layers of SEBS phantoms were created. The phantom was made of 2 parts, each layer had different acoustic and mechanical properties as a result of varying the concentration SEBS used or the gel. Thereafter the films were folded in order to create a branched vessel prototype. A solder was used to attach the ends together by melting a small part of the ends and then let it cool while attached.

The benefits obtained by the films is that one could fold the film and create different and more complex arterial shapes, such as bend, spiral and straight channels

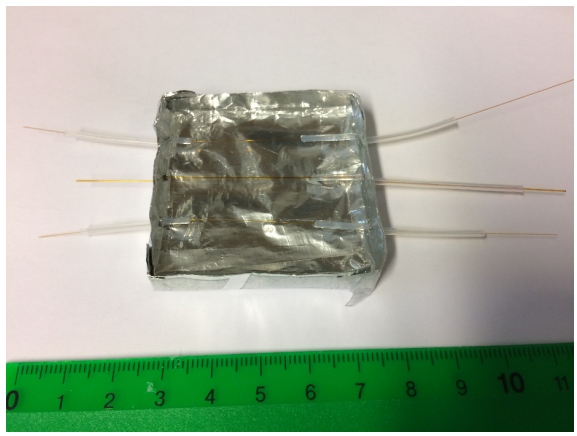

Figure 3.6: A mold for a simple vessel phantom can be seen, consisting of a handmade cubic mold using aluminum foil, and three different glass capillaries of different diameter. At the top of the image a 175 µm vessel glass capillary is used, the one in the middle is 375 µm and the last one is 150 µm. The plastic tubes seen are used to connect to lucer-lock syringes. The ruler is graded in centimeters.

3.11 Creating multi-layered phantoms

Phantom consisting of several layers were manufactured. In one test the ballistic gel was used as the protective coating layer, and SEBS was used as the direct surrounding tissue. Following the similar steps as in 3.10. Here two different gels were used. When the gels are melted and the mold is prepared, first the thin layer of ballistic gel is poured into the mold and left to cool down until solidification. Later the melted SEBS gel is poured upon it so that the capillaries are covered in it and again left to

cool down until solidification. The last step is to pour the last layer of melted ballistic gel, and left it cool . A quality test was performed to check the uniformity and the visibility of the vessel-like channels.

3.12 Flow evaluation of vessel phantoms

Figure 3.7 shows on of the phantoms used to check the flow through the vessels. A 5x6x3 cm phantom was fabricated in the same way as described in section 3.9. As seen in Figure 3.7, a plastic tube is used to ensure that the needles are kept in place. The following equipment used for evaluating the flow through vessel phantoms: A clinical ultrasound scanner (Philips Epiq 7), a mechanical pump, phantoms, water and a contrast agent. The test included taking ultrasound images to check the visibility of the micro, and testing flows of different velocities 5, 10, 20, and 100 µl/min.

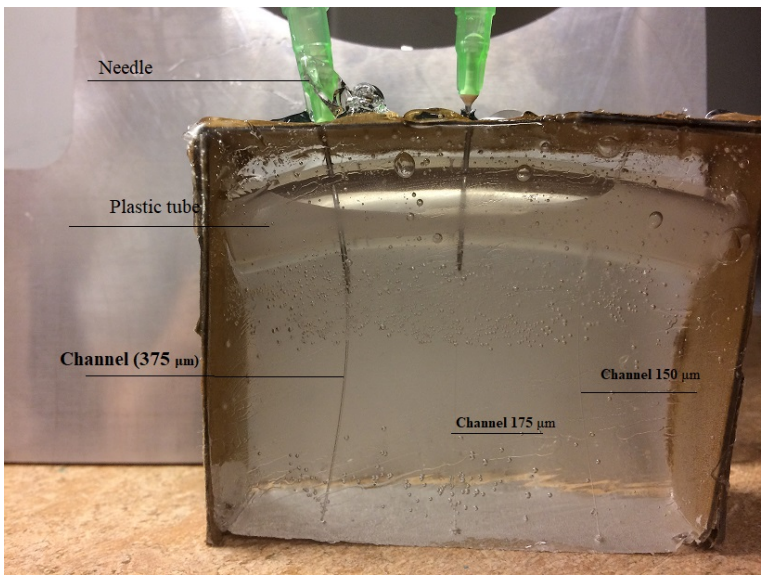

Figure 3.7: Flow phantom: The plastic tube is used to ensure that the needles stay in place. The phantom was fabricated same way as described in this study.

Chapter 4
Results

4.1 Speed of sound

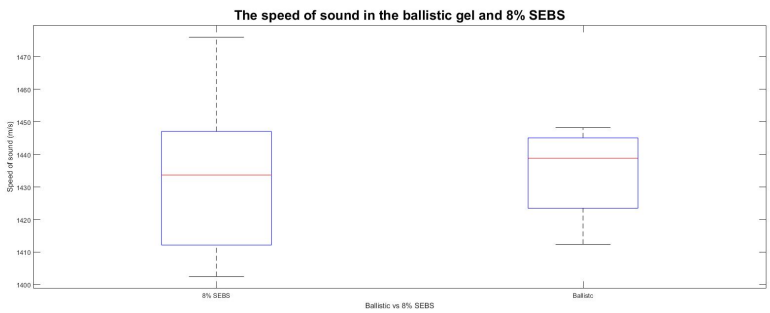

Figure 4.1: Boxplot giving the speed of sound measured for 8% SEBS and the clear ballistic gel. The red line delineates the median values.

The values of speed sound measured for both the 10% clear ballistic gel and 8% SEBS in mineral oil with the dynamic viscosity of 51.5 cp at a shear rate of 100 s^{-1} are seen in Figure 4.1. The mean speed of sound measured for 8% SEBS is 1433 m/s and for 10% clear ballistic gel is 1434 m/s.

Figure 4.2 shows the speed of sound measured for three sets of phantoms with 2%, 5% and 8% SEBS as concentrations in paraffin oil with the mean values of 1448.7, 1453.9 and 1458, 3 m/s, respectively.

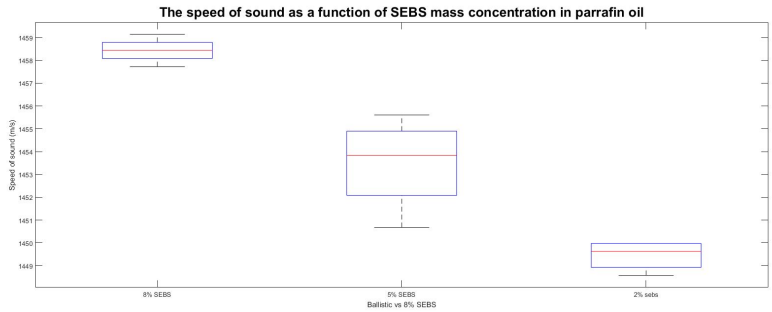

Figure 4.2: Boxplot of the speed of sound (m/s) as a function of SEBS mass concentration in paraffin oil. The red line delineates the median values, while the whiskers extend to the most extreme values which are not considered outliers.

4.2 Attenuation measurements

Material	Attenuation dB/MHz/cm
8% SEBS in mineral oil	0.83
Clear ballistic gel	0.40

Table 4.1: The attenuation estimated in dB/cm/MHz for SEBS and clear balistic gel.

Table 4.1 gives the attenuation for SEBS which was estimated to 0.83 dB/cm/MHz and the attenuation for clear ballistic gel was estimated to 0.40 dB/cm/MHz.

4.3 Elasticity measurements

The stress as a function of time, 6 minutes, is seen in Figure 4.3. The samples where held at constant length during this time.

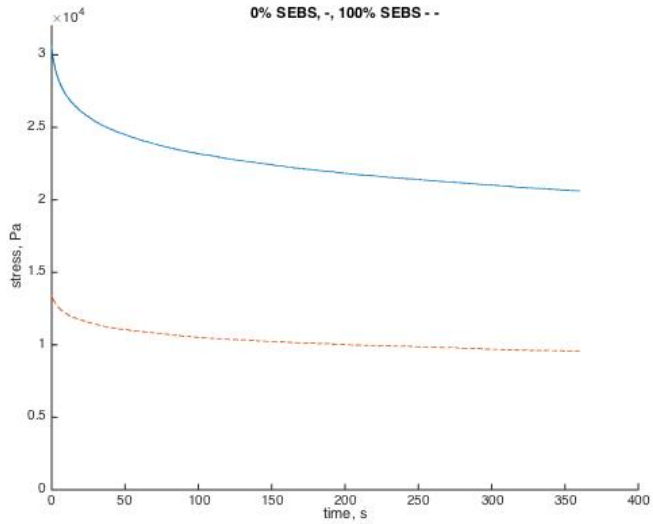

Figure 4.3: The stress (Pa) as a function of time (s) for 6 minutes as the sample is held at constant length.

4.4 Phantom materials

SEBS in mineral oil and ballistic gel with added glass beads were selected for the final phantom prototypes. The concentration of SEBS in mineral oil was decided depending on the tissue it would mimic. Furthermore, SEBS was selected due to its properties regarding mechanical stability and also durability. SEBS released easily from the molds used. The Clear Ballistic gel was chosen to mimic the outer layer of the artery. PDMS was not used, since it was impossible to withdraw the capillaries out from the phantoms.

4.5 Developed phantom molds

In order to produce multi-layered vessel phantoms a mold of five parts was printed, see Figure 4.4. The main reason for using these molds was to produce the vessel phantom of the desired shape and geometry. The surrounding structure was cast in a mold made of cardboard.

Using so many parts made it easier to extract the phantom when cured. Electrical tape was used to assemble the mold.

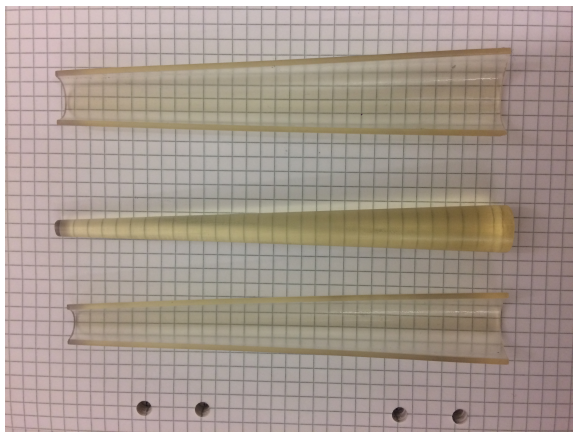

Figure 4.4: Mold for vessel phantom consisting of five parts, only three are shown. At the top of the image on of two identical parts of the first outside contour can be seen,. In the middle of the image the inner contour is seen. Below in the image is one of two identical part of the second outside contour.

4.6 Developed vessel phantoms

Figure 4.5 shows a simple vascular ultrasound phantom. The phantom contained a 150, 175, 375 µm simulated vessel at varying depth. The plastic tubes are needed for the connection to a standard lucer-lock syringe.

As mentioned in section 3.9; Two different ultrasound phantom materials were investigated. PDMS and 8% SEBS. However, trying to withdraw the glass capillaries out of the PDMS phantom failed. This was not the case with the phantom made of SEBS where the withdrawing of the capillaries was easily done.

5, 10, 20, and 100 µl/min water flow through the vessels were evaluated. Figure 4.6 shows three ultrasound images of a 375 µm in diameter channel, the channel were fully visible with no bubbles.

The 150 µm in diameter channel was seen and a flow of water went through. The water was injected by hand and a diameter change was noticed, as seen in Figure 4.8.

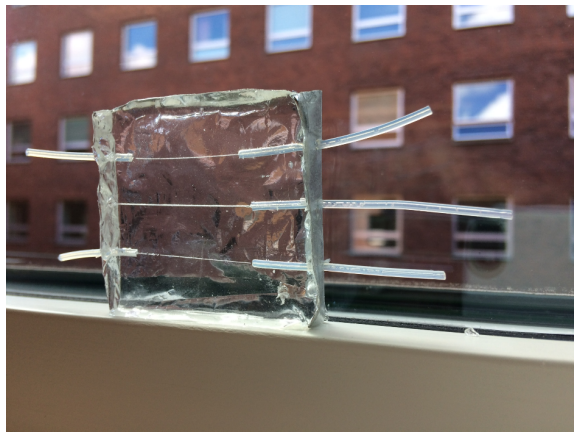

Figure 4.5: An image of the final phantom, with 150, 175, 375 µm vessel like channels from the top down.

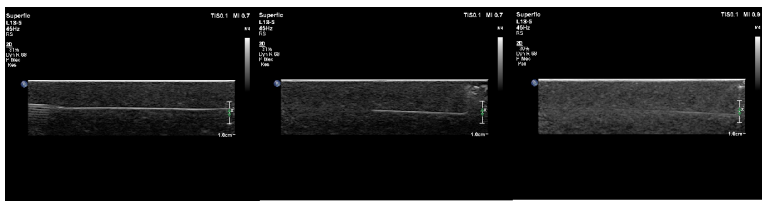

Figure 4.6: Ultrasound images indicating that capillary channels are seen via ultrasound. The image to the left was taken before injecting water 20 µl/min though, the one in the middle was taken when the channel was half filled and in the last image the channel is filled. Artifact from the needle is seen image to the left

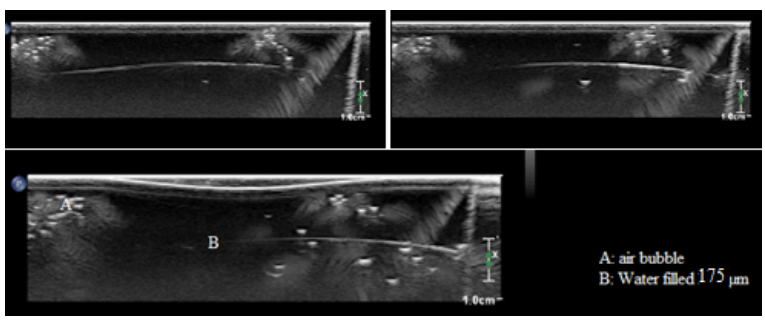

Figure 4.7: A 175 µm in diameter channel is seen. The image at the top-left was taken before injecting water, the one on the top-right was taken when the channel was injected (20 µl/min) and the last image indicates artifacts in the channel, probably due to air bubble.

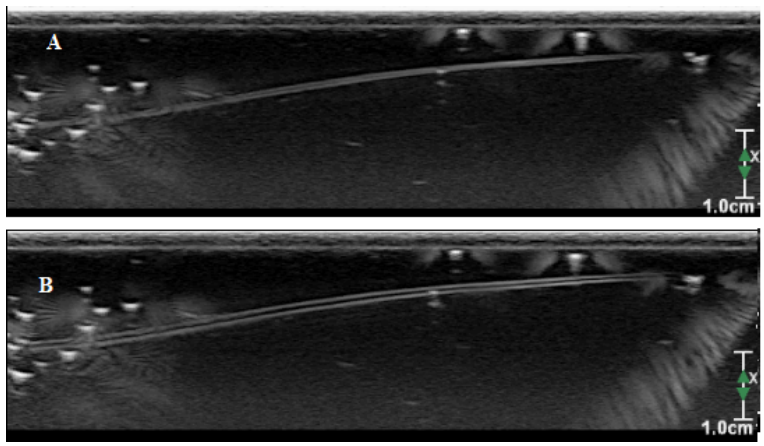

Figure 4.8: Ultrasound images of a 150 µm in diameter channel. Water was injected by hand in sequences which results in a shape change of the channel. A shows the micro channel during a low water flow compared to the water flow in B.

4.7 Developed vessel phantoms exhibiting the longitudinal movement

The phantom exhibiting longitudinal movement consists of three different layers. The first layer was made of 8% SEBS with added glass beads, 7 g/liter, representing the intima-media complex and its *vasa vasorum*. The second layer was made of 5% SEBS and with added glass beads, 5 g/liter. The third layer was made of 8% SEBS with added glass beads, 4 g/liter, mimicking the adventitia and the surrounding tissue. Figure 4.9 shows a schematic drawing of how the phantom layers are placed.

The first and the second layer of the phantom were 2 mm thick each, see Figure 4.10 and were the most the critical; they were easy to break and bubbles could get trapped while manufacturing. The vessel phantom with its *vasa vasorum* was designed in one version. As seen in Figure 4.9, the inner diameter of the vessel is decreasing gradually. The phantom was 15 cm long and with a height of 8 cm. The outer diameter of the vessel phantom is approximately the same size as the diameter of the human aorta.

A 175 µm channel representing the *vasa vasorum* was placed in the intima-media complex layer.

After cutting the third and surrounding part, see Figure 4.11, in two halves a heat gun was used to slightly heat up the inner surface of it. Thereafter the vessel phantom was placed inside and the final phantom was assembled.

Finally, the phantom was connected to the pump and the wall movements were measured, using the same method used in [28]. Figure 4.13 shows the ultrasound images for

The longitudinal wall movement was measured to 0.2 mm and the radial movement to 0.8 mm.

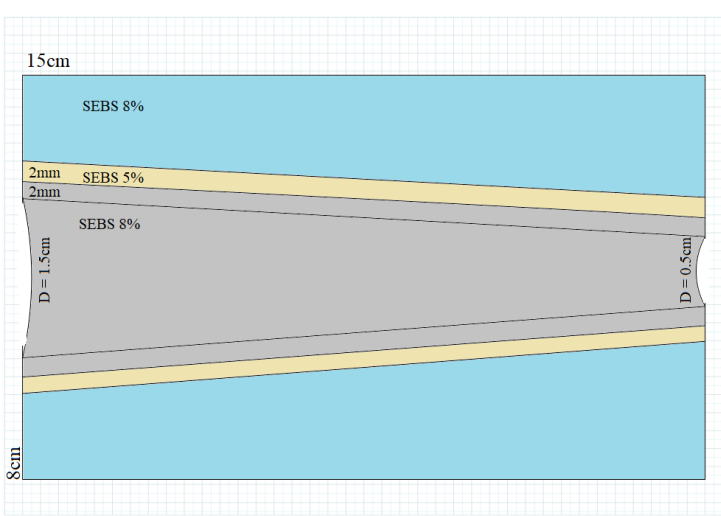

Figure 4.9: Section of the phantom; the intima-media complex (gray),connective tissue (yellow), the adventitia and the surrounding tissue (blue).

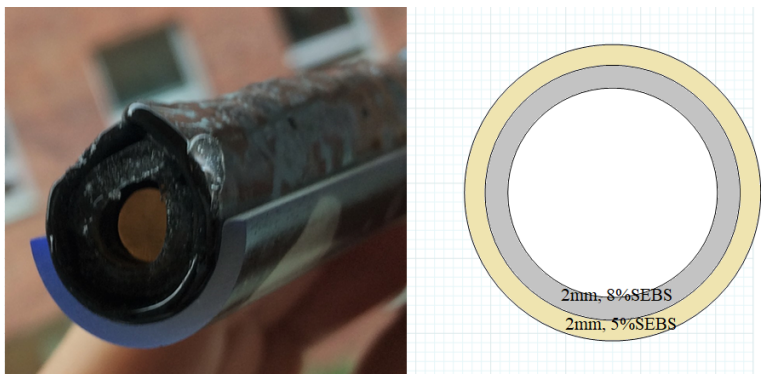

Figure 4.10: Left, the two layered vessel phantom before placing in the third - surrounding- part of the phantom. Right a cross-sectional view of the vessel phantom.

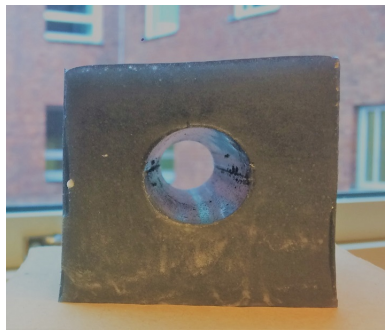

Figure 4.11: An image of the third and surrounding part of the phantom.

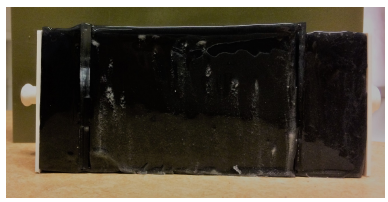

Figure 4.12: An image of the final phantom exhibiting the longitudinal movement.

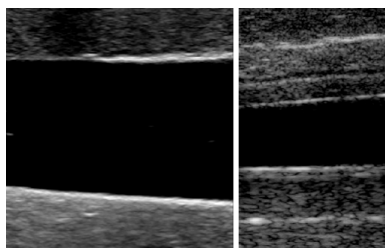

Figure 4.13: Ultrasound images, the image on the left was taken before placing the capillary in place and the image on the right is the final phantom exhibiting the longitudinal movement.

Chapter 5
Discussion

The aims defined in section 1.1 involve testing different tissue mimicking materials, design and fabrication of vessel-like phantoms and investigating these phantoms using ultrasound imaging.

Firstly, a literature study of different tissues mimicking materials was conducted. Many soft tissues mimicking material have been described in table 2.6. The main focus has been to suggest a material that can best mimic the mechanical and acoustic properties of the living vessel wall layers.

Agarose-based materials have been well documented and frequently used as a soft tissue phantom material. They have the advantage that they are easy to manufacture and their acoustic properties can be tailored. However, phantoms made of agarose have to be handled very carefully since the material is very delicate and easy to break. Polyvinyl alcohol, like agaroes can be acoustically tailored and is an excellent choice for manufacturing more complex phantoms. However, they suffer from having poor longevity and requires multiple freeze-thaw cycles. Of the remaining soft tissue substitutes described in table 2.6, each is limited either by its mechanical properties, longevity or acoustic proprieties.

Numerous tissue phantoms such as SEBS in mineral oil and ballistic gel are available commercially and described in sections 2.13 and 2.14. Ballistic and SEBS gels both have the advantages that they are simple to prepare, have acoustic and mechanical properties similar to those for soft tissue. Combining SEBS polymer and mineral oil provided an efficient way of developing tissue mimicking material with customized properties. Furthermore, the ability to combine SEBS and ballistic materials is an additional and efficient way towards three-layered vessel-like phantom models. Given these points, SEBS and ballistic gels were selected for further investigation.

The preparation of SEBS gel was relatively easy, and the same goes for ballistic gel. However, air bubbles sometimes could be produced during phantom manufacturing, leaving a hole. This problem was solved by heating the gel to at least 130° and slowly

pouring it into the mold. The added glass beads which serve as scatters were not distributed uniformly but good enough to be used.

The mechanical properties of the selected phantom tissue mimicking materials for the ultrasound phantoms developed during this work were tested. Results from measuring the stress as a function of time for the Ballistic gel and 8% SEBS a are shown in Figure 4.3. According to [61], an increase in the SEBS copolymer concentrations results in an increase in the stiffness of the gel as well as in speed of sound. However, in this work, the mechanical properties for 8% SEBS and ballistic gel were tested, and the reason was that 2 and 4% SEBS phantoms were soft and therefore difficult to be tested using the tensile test machine used in this study. As described in section 2.1 the main constituents of vascular tissue are elastin, collagen fibers and smooth muscle cells, where each has a specific Young's modulus. Additionally, each artery walls consists of primary three layers that differ from each other both morphologically and biologically. Due to these complex properties, it is unmanageable to define Young's modulus as can be done in the way it is measured for tissue mimicking materials. Still, in order to obtain a global idea of the vascular wall mechanics, it is possible to merge all the properties together and treat each of the vascular wall layer as if it is homogeneous. The decision made was that the intima-media-complex-like phantom layer should have a lower stiffness than the surrounding tissue which included the adventitia layer and should be as elastic as muscles and that both layers should be connected to each other with a material that is more elastic/softer simulating connective tissue.

The results from measuring the speed of sound can be seen in Figures 4.1 and 4.2. When comparing these results with table 2.2, it is noticed that the speed of sound is slightly lower than in soft tissue. Additionally, when using paraffinic oil as a plasticizer an increase in the speed of sound is observed, this can be due to the difference in oil viscosity as described by Cabrelli et al. [40]. The attenuation for SEBS was estimated to 0.83 dB/cm/MHz and almost mimicked the muscles, see table 2.3. This was not the case for the ballistic gel which was estimated to 0.40 dB/cm/MHz. However, these values may be not valid and the reason behind this speculation is that when measuring the attenuation two assumptions were made; the attenuation in the phantom material was assumed to be linearly dependent on frequency and that no sound waves were attenuated in water. In future work, in order to get more accurate results more measurements using for e.g, multiple narrow-band transducers covering a wider range of frequencies is needed.

Phantoms manufacturing include the design and fabrication of different molds. The materials of which the molds are to be fabricated should be suitable; meaning that the phantom is easy to release from the mold. Since SEBS and ballistic gels are oil based gels, a mold made of hydrophilic materials should be ideal. This was only investigated on materials in-house, such as PDMS and PVA-molds, PMMA, brass and glass by comparing the ease the phantoms were released from molds made of

the mentioned materials. However, in order to fully investigate such behavior more accurate experiments have to be done. Results from checking the contact angle of a drop of water or oil on each material-surface can suggest the ideal mold material.

The second and main focus of this project has been to design phantoms that simulate the *vasa vasarum*, and methods to construct the phantoms. Using SEBS and ballistic gel several vessel-like phantoms with different complexity were fabricated.

Figure 4.5 shows one phantom prototype. A wall-less vessel phantom, simulating vessels of different diameters, 150, 175 and 375 µm are shown. SEBS, ballistic gel or a combination of both could be used to manufacture this phantom. Additionally, the design and fabrication steps of such phantoms do not include the use of 3D printed molds which makes the fabrication steps relatively easy. The fabricated channels diameters are in good agreement with the vessels diameters data obtained from the literature, see Figure 2.4. Figures 4.8, 4.7, 4.6 showed that it was possible to detect a flow through the channels using ultrasound techniques. However, one common problem was having the needles in place and not cutting through the gels. This was solved bu using a plastic tube as described in section 3.12.

Equations 2.1, 2.2, 2.3 and 2.4 show that there are several parameters which influence the flow dynamic within *vasa vasorum*, such as the radius, the pressure and the velocity. Therefore, to obtain wall-less vessel phantoms and *vasa vasorum* that are consistent with the realistic vessels, these relationships are of interest and should be experimentally verified.

The walled and multi-layered vessel design consists of several steps: first, manufacturing two thin films and a supportive thick structure; an inner layer in which a *vasa vasarum* channel-like is implemented, a connective layer and an outer covering and supporting layer. Second, folding the thin layers around each other to form a cylinder with a decreasing diameter. Third, placing the vessel-mimicking phantom inside the supporting structure. Figure 4.9 shows a longitudinal section view and portrays the phantom exhibiting longitudinal as well as radial movements. the *vasa vasorum* channel like was placed in the inner layer of the vessel. The phantom was tested and the longitudinal movement was measured to 0.2 mm whilst the radial movement to 0.8 mm. As mentioned in section 2.2 the arterial wall longitudinal movement has been measured to 0.1-1 mm which is of the same magnitude as the radial movement. The wall movements of the phantom developed during this work were not of the same magnitudes. In the previously developed phantoms made of PVA, also mentioned in section 2.2, the wall movements were of the same magnitude. Additionally, as observed, the phantoms surrounding structure was less elastics than the surrounding structure fabricated in the previous work, which can explain the differences in wall movements measured.

In Appendix 7.0.2, additional work have been done in order to investigate other possibilities arise from mixing SEBS in mineral oil as well as ballistic gels offers. A

branched multi-layered vessel phantom prototype have been designed and manufactured. The result showed that these two gels are excellent alternatives to other existing tissue mimicking materials. However, if more complex vessel shapes are of interest a 3D printer might be required. Moreover, it is strongly believed that other ultrasound phantom, such as breast tumors which can be used for biopsy training, are possible to produce using these materials, see Future work 6.0.1.

Chapter 6
Conclusion

To summarize, during this work several vessel-like ultrasound phantom prototypes have been designed and fabricated. SEBS mixtures and ballistic gels have shown to be perfect vessel tissue mimicking material.

The phantoms were made of SEBS or ballistic gels. Some of the designs steps suggested did not include the use of a 3D printer and both wall-less, as well as walled and multi-layered vessel, were introduced. *vasa vasorum*-like channels of diameters 150, 175 and 375 µm were fabricated, checked by ultrasound and the flow through these phantoms was evaluated.

The phantom materials used were investigated, the acoustic and mechanical properties were measured and the results were in good agreement with data obtained from the literature. The final phantom exhibiting the longitudinal movement was made of three layers. An inner layer made of 8% SEBS with added glass beads to ensure strong and enough echoes in ultrasound images needed to track the movement. A *vasa vasorum*-like channel was placed in this layer. The second layer had a fat-like elasticity and was used as connective tissue between the inner and the outer layer. The third layer mimicked the soft tissue surrounding vessels. A wall motion, longitudinally and radially, was produced. However, these motions did not mimic wall motions in a living vessel. To solve this issue, it is suggested to investigate the influence of using a stiffer phantom material as surrounding layer.

However, in living vessels, the morphology, as well as the biology, is too complex to be fully mimicked by tissue mimicking material.

6.0.1 Future work

Potential improvements to the present work will be highlighted here, categorized as improvements to the geometry and design, as well as additional improvements specifically to tissue mimicking material.

More complex vessel geometries are of interest to investigate, therefore more flexible molds have to be designed and manufactured. Both PVA and PDMS are water-based materials. In one test, two molds, one made of PVA and another of PDMS were made. the phantoms were released easily from both molds. Furthermore, using a 3D printer, more complex mold shapes can be produced. SEBS and ballistic gels offer limitless possibilities in the world of ultrasound phantom making. However, more has to be done in order to investigate the acoustic and mechanical properties of different SEBS blends as well as ballistic gel.

For this particular work; vessel phantom layers of SEBS blends and ballistic gels of different elasticity are used. Suggesting a way to measure the tensile strength of each layer could be useful in order to better compare with literature data regarding Young's modulus for different vessel layer tissues.

Chapter 7
Appendices

7.0.1 Appendix A

The Matlab code below does two things: it phase-inverses the back reflected signal and runs a cross-correlation between the front and the back reflected signals, as seen in Figure 3.4. The reason behind this is that when an ultrasound wave goes from a material with an acoustic impedance Z_1 into a second material with a lower acoustic impedance Z_2, it undergoes phase inversion. The cross-correlation of the two echo curves is to check how well the two curves fit each other. Figure 7.2 shows the results from two cross-correlated echo curves.

The cross-correlation was performed by using (Matlab, MathWorks, Natick, MA, USA) code.

section*A novel and affordable SEBS co-polymer in mineral oil phantom model for training in ultrasound-guided vascular access

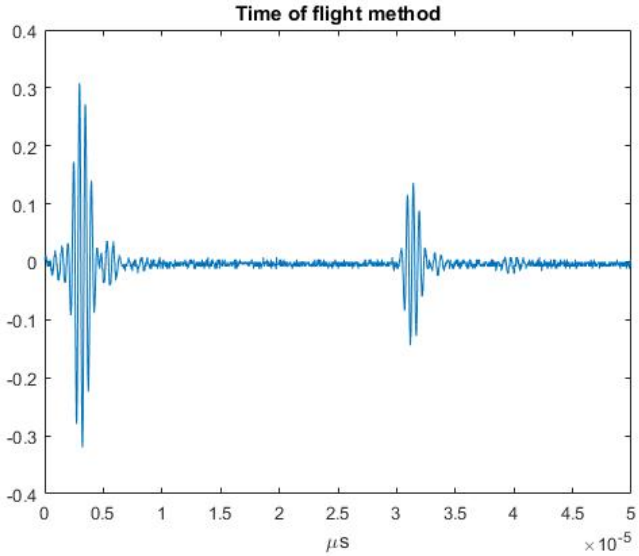

Figure 7.1: Echoes for the estimation of speed of sound in the phantom at 21°C as seen on the oscilloscope screen.

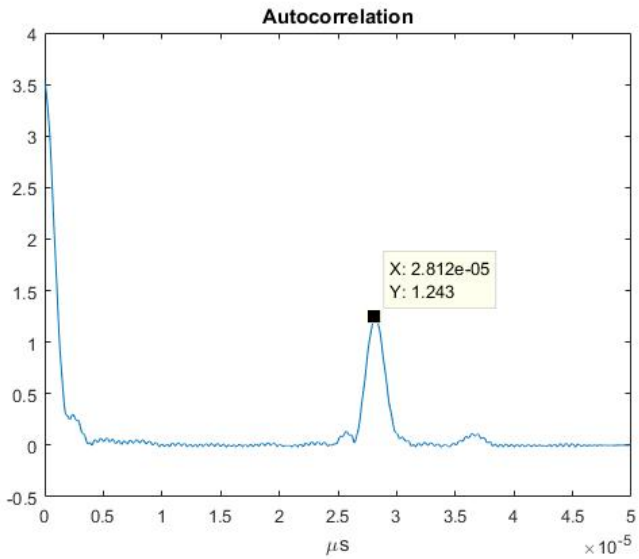

Figure 7.2: The result from the Cross-correlation between the echos. in this particular test, the time delay was estimated to 2.81e-05 µs.

```
clear

% Load the file
seq = openfile('TEK0025.CSV');
% Remove the offset from time scale
seq(:,1) = seq(:,1)-seq(1,1);

% Plot sequence
figure
plot(seq(:,1), seq(:,2))
title('Time of flight method')
xlabel('\mus')

% Calculate correlation between signal and phase inverted signalx
c = xcorr(seq(:,2),-seq(:,2));
% Extract the envelop from correlation
d = envelope(c);
% Shift signal to get major peak at origin
% Plot result
d = fftshift(d);

% Find peak
[value,loc] = findpeaks(d(1:length(seq)),seq(:,1),'MinPeakProminence',10);

% Plot autocorrelation
figure
plot(seq(:,1),d(1:length(seq)))
title('Autocorrelation')
xlabel('\mus')
hold on
plot([loc;loc],[0;value],'k--')
```

7.0.2 Appendix B

A branched multi-layerd vessel phantom portotype

In this section, a branched multi-layered vessel phantom is fabricated. Firstly, thin filmss of 8% SEBS in paraffin oil were manufactured. For more manufacturing details, see sections 3.2 and 3.10

The films were folded and fused together as shown in Figure 7.3, d, using a heat solder. After manufacturing the branched vessel, more gel with was poured on. Differences in the scatters concentration or/and SEBS concentration between the branched vessel and the surrounding gel is what makes possible creation of walled vessel-like channels.

The final phantom was checked with an ultrasound, images are seen in Figure 7.3, a, b, c.

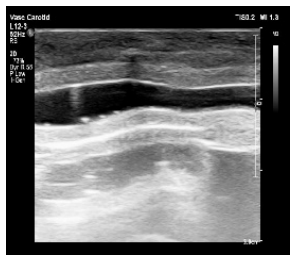

(a) An ultrasound image of the vessel phantom simulation a vessel with a plaque.

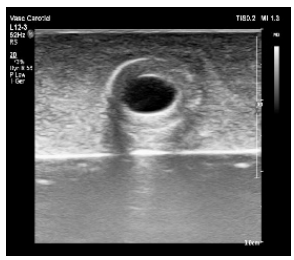

(b) An ultrasound image of the walled-vessel phantom.

(c) An image of the walled-vessel phantom, deformed shape.

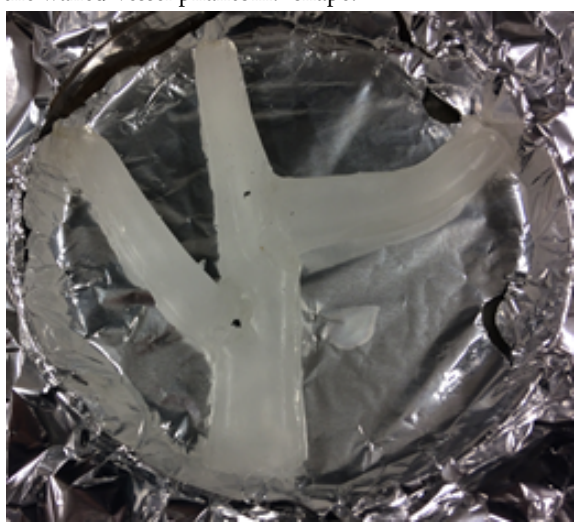

(d) An image of the walled-vessel phantom, deformed shape.

Figure 7.3: An image of a branched vessels phantom prototype and ultrasound images.

References

[1] WHO, "World health organization." http://www.who.int/mediacentre/factsheets/fs317/en, 2017.

[2] C. ANZICS, "Centre for outcome and resource evaluation annual report 2011–2012," *Australian and New Zealand Intensive Care Society, Melbourne*, 2013.

[3] M. Lawlor, B. Gersh, L. Opie, and T. A. Gaziano, "The global perspective of ischemic heart disease," *Chronic Coronary Artery Disease: A Companion to Braunwald's Heart Disease E-Book*, p. 16, 2017.

[4] M. Sznajder, P. Aegerter, R. Launois, Y. Merliere, B. Guidet, and V. CubRea, "A cost-effectiveness analysis of stays in intensive care units," *Intensive Care Medicine*, vol. 27, pp. 146–153, Jan 2001.

[5] J. Graf, C. Mühlhoff, G. S. Doig, S. Reinartz, K. Bode, R. Dujardin, K.-C. Koch, E. Roeb, and U. Janssens, "Health care costs, long-term survival, and quality of life following intensive care unit admission after cardiac arrest," *Critical Care*, vol. 12, p. R92, Jul 2008.

[6] J.-L. Vincent, "Fluid management: the pharmacoeconomic dimension," *Critical Care*, vol. 4, p. S33, Oct 2000.

[7] Hjärt-lungfoden, "Hjärtinfarkt -vad är det?." https://www.hjart-lungfonden.se/Sjukdomar/, 2016.

[8] . Purwanto, C. Eswaran, R. Logeswaran, and A. R. A. Rahman, "Prediction models for early risk detection of cardiovascular event," *Journal of Medical Systems*, vol. 36, pp. 521–531, Apr 2012.

[9] A. H. Nicholas, R. N. Spooner-Hart, and R. A. Vickers, "Abundance and natural control of the woolly aphid eriosoma lanigerum in an australian apple orchard ipm program," *BioControl*, vol. 50, no. 2, pp. 271–291, 2005.

[10] M. Cinthio, Å. R. Ahlgren, J. Bergkvist, T. Jansson, H. W. Persson, and K. Lindström, "Longitudinal movements and resulting shear strain of the arterial wall," *American Journal of Physiology-Heart and Circulatory Physiology*, vol. 291, no. 1, pp. H394–H402, 2006.

[11] M. Cinthio, A. R. Ahlgren, T. Jansson, A. Eriksson, H. W. Persson, and K. Lindstrom, "Evaluation of an ultrasonic echo-tracking method for measurements of arterial wall movements in two dimensions," *IEEE Transactions on Ultrasonics, Ferroelectrics, and Frequency Control*, vol. 52, pp. 1300–1311, Aug 2005.

[12] M. Cinthio, Å. R. Ahlgren, J. Bergkvist, T. Jansson, H. W. Persson, and K. Lindström, "Longitudinal movements and resulting shear strain of the arterial wall," *American Journal of Physiology - Heart and Circulatory Physiology*, vol. 291, no. 1, pp. H394–H402, 2006.

[13] Å. R. Ahlgren, M. Cinthio, S. Steen, T. Nilsson, T. Sjöberg, H. W. Persson, and K. Lindström, "Longitudinal displacement and intramural shear strain of the porcine carotid artery undergo profound changes in response to catecholamines," *American Journal of Physiology - Heart and Circulatory Physiology*, vol. 302, no. 5, pp. H1102–H1115, 2012.

[14] D. Staub, M. B. Patel, A. Tibrewala, D. Ludden, M. Johnson, P. Espinosa, B. Coll, K. A. Jaeger, and S. B. Feinstein, "Vasa vasorum and plaque neovascularization on contrast-enhanced carotid ultrasound imaging correlates with cardiovascular disease and past cardiovascular events," *Stroke*, vol. 41, no. 1, pp. 41–47, 2010.

[15] M. Gössl, M. Rosol, N. M. Malyar, L. A. Fitzpatrick, P. E. Beighley, M. Zamir, and E. L. Ritman, "Functional anatomy and hemodynamic characteristics of vasa vasorum in the walls of porcine coronary arteries," *The anatomical record*, vol. 272, no. 2, pp. 526–537, 2003.

[16] G. Zahnd, D. Vray, A. Sérusclat, D. Alibay, M. Bartold, A. Brown, M. Durand, L. M. Jamieson, K. Kapellas, L. J. Maple-Brown, *et al.*, "Longitudinal displacement of the carotid wall and cardiovascular risk factors: associations with aging, adiposity, blood pressure and periodontal disease independent of cross-sectional distensibility and intima-media thickness," *Ultrasound in medicine & biology*, vol. 38, no. 10, pp. 1705–1715, 2012.

[17] J. K. Williams and D. D. Heistad, "Structure and function of vasa vasorum," *Trends in cardiovascular medicine*, vol. 6, no. 2, pp. 53–57, 1996.

[18] Z.-Z. Song and Y.-M. Zhang, "Contrast-enhanced ultrasound imaging of the vasa vasorum of carotid artery plaque," *World journal of radiology*, vol. 7, no. 6, p. 131, 2015.

[19] A. H. Pereira, "Rupture of vasa vasorum and intramural hematoma of the aorta: a changing paradigm," *Jornal Vascular Brasileiro*, vol. 9, no. 2, pp. 57–60, 2010.

[20] M. O. Culjat, D. Goldenberg, P. Tewari, and R. S. Singh, "A review of tissue substitutes for ultrasound imaging," *Ultrasound in medicine & biology*, vol. 36, no. 6, pp. 861–873, 2010.

[21] E. L. Ritman and A. Lerman, "The dynamic vasa vasorum," *Cardiovascular research*, vol. 75, no. 4, pp. 649–658, 2007.

[22] J. Humphrey and S. Na, "Elastodynamics and arterial wall stress," *Annals of biomedical engineering*, vol. 30, no. 4, pp. 509–523, 2002.

[23] D. Miranda, "vasa vasorum." `https://clinanat.com/100-mtd/358-vasa-vasorum`, 2017.

[24] A. Portanova, N. Hakakian, D. J. Mikulis, R. Virmani, W. M. Abdalla, and B. A. Wasserman, "Intracranial vasa vasorum: insights and implications for imaging," *Radiology*, vol. 267, no. 3, pp. 667–679, 2013.

[25] F. Lindgärde, T. Thulin, and J. Östergren, *Kärlsjukdom : vaskulär medicin.* Lund : Studentlitteratur, 2009 (Ungern), 2009.

[26] H. W. P. K. L. J. A. T. N. S. S. Magnus Cinthio, Åsa Rydén Ahlgren, "Longitudinal movement of the arterial wall (in detail)." `http://bme.lth.se/research-pages/ultrasound/research/ultrasound-methodologies-for-cardiovascular-research/longitudinal-movement-of-the-arterial-wall/longitudinal-movement-of-the-arterial-wall-in-detail/`, 2015.

[27] Å. R. Ahlgren, M. Cinthio, H. W. Persson, and K. Lindström, "Different patterns of longitudinal displacement of the common carotid artery wall in healthy humans are stable over a four-month period," *Ultrasound in medicine & biology*, vol. 38, no. 6, pp. 916–925, 2012.

[28] S. Sjöstrand, A. Widerström, Å. R. Ahlgren, and M. Cinthio, "Design and fabrication of a conceptual arterial ultrasound phantom capable of exhibiting longitudinal wall movement," *IEEE transactions on ultrasonics, ferroelectrics, and frequency control*, vol. 64, no. 1, pp. 11–18, 2017.

[29] Z. Sun, "Atherosclerosis and atheroma plaque rupture: normal anatomy of vasa vasorum and their role associated with atherosclerosis," *The Scientific World Journal*, vol. 2014, 2014.

[30] R. Scotland, P. Vallance, and A. Ahluwalia, "On the regulation of tone in vasa vasorum," *Cardiovascular research*, vol. 41, no. 1, pp. 237–245, 1999.

[31] O. CNX, "Anatomy and physiology." `https://cnx.org/contents/14fb4ad7-39a1-4eee-ab6e-3ef2482e3e22@8.25`, 2017.

[32] F. W. Kremkau, *Diagnostic ultrasound: principles and instruments*. WB Saunders Company, 2001.

[33] P. R. Hoskins, K. Martin, and A. Thrush, *Diagnostic ultrasound: physics and equipment*. Cambridge University Press, 2010.

[34] J. Vincent, "Basic elasticity and viscoelasticity," *Structural Biomaterials*, pp. 1–28, 2012.

[35] J. F. Vincent, *Structural biomaterials*. Princeton University Press, 2012.

[36] J. W. Pepi, "Linear analysis using secants for materials with temperature dependent nonlinear elastic modulus and thermal expansion properties," in *Optomechanical Engineering 2017*, vol. 10371, p. 1037108, International Society for Optics and Photonics, 2017.

[37] E. L. Madsen, J. A. Zagzebski, R. A. Banjavie, and R. E. Jutila, "Tissue mimicking materials for ultrasound phantoms," *Medical physics*, vol. 5, no. 5, pp. 391–394, 1978.

[38] E. L. Madsen, G. R. Frank, and F. Dong, "Liquid or solid ultrasonically tissue-mimicking materials with very low scatter," *Ultrasound in medicine & biology*, vol. 24, no. 4, pp. 535–542, 1998.

[39] J. Ophir, N. F. Maklad, and P. M. Jaeger, "Ultrasound phantom," Sept. 1 1981. US Patent 4,286,455.

[40] L. C. Cabrelli, F. W. Grillo, D. R. Sampaio, A. A. Carneiro, and T. Z. Pavan, "Acoustic and elastic properties of glycerol in oil-based gel phantoms," *Ultrasound in Medicine and Biology*, vol. 43, no. 9, pp. 2086–2094, 2017.

[41] H. Kosukegawa, K. Mamada, K. Kuroki, L. Liu, K. Inoue, T. Hayase, and M. Ohta, "Measurements of dynamic viscoelasticity of poly (vinyl alcohol) hydrogel for the development of blood vessel biomodeling," *Journal of Fluid Science and Technology*, vol. 3, no. 4, pp. 533–543, 2008.

[42] K. Zell, J. Sperl, M. Vogel, R. Niessner, and C. Haisch, "Acoustical properties of selected tissue phantom materials for ultrasound imaging," *Physics in medicine and biology*, vol. 52, no. 20, p. N475, 2007.

[43] N. R. Legge, "Thermoplastic elastomers," *Rubber Chemistry and Technology*, vol. 60, no. 3, pp. 83–117, 1987.

[44] C. M. Koo, "Electroactive thermoplastic dielectric elastomers as a new generation polymer actuators," in *Thermoplastic Elastomers*, InTech, 2012.

[45] A. S. Esposito, "High strength elastomers for pharmaceutical products," Mar. 21 1989. US Patent 4,814,375.

[46] L. C. Cabrelli, P. I. Pelissari, A. M. Deana, A. A. Carneiro, and T. Z. Pavan, "Stable phantom materials for ultrasound and optical imaging," *Physics in medicine and biology*, vol. 62, no. 2, p. 432, 2016.

[47] F. W. Grillo, L. C. Cabrelli, L. T. Ribeiro, T. Z. Pavan, A. A. Carneiro, R. D. Herculano, and F. A. Borges, "White-silicone rubber and copolymer-in-oil blend for ultrasound soft tissue mimicking material," in *Ultrasonics Symposium (IUS), 2017 IEEE International*, pp. 1–4, IEEE, 2017.

[48] C. Ballistic, "About ballistic gelatin." `https://www.clearballistics.com/faq/`, 2017.

[49] R. Amini, J. Z. Kartchner, L. A. Stolz, D. Biffar, A. J. Hamilton, and S. Adhikari, "A novel and inexpensive ballistic gel phantom for ultrasound training," *World journal of emergency medicine*, vol. 6, no. 3, p. 225, 2015.

[50] D. S. Morrow, J. A. Cupp, and J. S. Broder, "Versatile, reusable, and inexpensive ultrasound phantom procedural trainers," *Journal of Ultrasound in Medicine*, vol. 35, no. 4, pp. 831–841, 2016.

[51] K. G. Nathan Boor, "Photo of synthetic ballistic gelatin showing terminal fragmentation of a .243 projectile," 2013. [[CC BY-SA 3.0 (https://creativecommons.org/licenses/by-sa/3.0)],Online; accessed 24,112017].

[52] T. L. Poepping, H. N. Nikolov, M. L. Thorne, and D. W. Holdsworth, "A thin-walled carotid vessel phantom for doppler ultrasound flow studies," *Ultrasound in medicine & biology*, vol. 30, no. 8, pp. 1067–1078, 2004.

[53] J. K. Tsou, J. Liu, A. I. Barakat, and M. F. Insana, "Role of ultrasonic shear rate estimation errors in assessing inflammatory response and vascular risk," *Ultrasound in medicine & biology*, vol. 34, no. 6, pp. 963–972, 2008.

[54] J. K. Tsou, J. Liu, A. I. Barakat, and M. F. Insana, "Role of ultrasonic shear rate estimation errors in assessing inflammatory response and vascular risk," *Ultrasound in medicine & biology*, vol. 34, no. 6, pp. 963–972, 2008.

[55] P. R. Hoskins, "Simulation and validation of arterial ultrasound imaging and blood flow," *Ultrasound in medicine & biology*, vol. 34, no. 5, pp. 693–717, 2008.

[56] K. Funamoto, O. Yamashita, and T. Hayase, "Poly (vinyl alcohol) gel ultrasound phantom with durability and visibility of internal flow," *Journal of Medical Ultrasonics*, vol. 42, no. 1, pp. 17–23, 2015.

[57] Y. Law, K. Johnston, H. Routh, and R. Cobbold, "On the design and evaluation of a steady flow model for doppler ultrasound studies," *Ultrasound in medicine & biology*, vol. 15, no. 5, pp. 505–516, 1989.

[58] C. J. Teirlinck, R. A. Bezemer, C. Kollmann, J. Lubbers, P. R. Hoskins, P. Fish, K.-E. Fredfeldt, and U. G. Schaarschmidt, "Development of an example flow test object and comparison of five of these test objects, constructed in various laboratories," *Ultrasonics*, vol. 36, no. 1-5, pp. 653–660, 1998.

[59] W. Dabrowski, J. Dunmore-Buyze, R. Rankin, D. Holdsworth, and A. Fenster, "A real vessel phantom for imaging experimentation," *Medical physics*, vol. 24, no. 5, pp. 687–693, 1997.

[60] D. M. King, C. M. Moran, J. D. McNamara, A. J. Fagan, and J. E. Browne, "Development of a vessel-mimicking material for use in anatomically realistic doppler flow phantoms," *Ultrasound in medicine & biology*, vol. 37, no. 5, pp. 813–826, 2011.

[61] J. Oudry, C. Bastard, V. Miette, R. Willinger, and L. Sandrin, "Copolymer-in-oil phantom materials for elastography," *Ultrasound in medicine & biology*, vol. 35, no. 7, pp. 1185–1197, 2009.